Controlling superconductivity of CeIrIn5 microstructures by substrate selection

van Delft, Maarten R.
Bachmann, M. D.
Putzke, Carsten
Guo, Chunyu
Straquadine, Joshua A.W.
Bauer, Eric Dietzgen
Ronning, Filip
Moll, Philip J W

To be published in: Applied Physics Letters

DOI to publisher's version: 10.1063/5.0082561

Applied Physics Letters

Controlling superconductivity of $CeIrIn_5$ microstructures by substrate selection

Cite as: Appl. Phys. Lett. **120**, 092601 (2022); https://doi.org/10.1063/5.0082561
Submitted: 16 December 2021 • Accepted: 15 February 2022 • Published Online: 02 March 2022

Maarten R. van Delft, Maja D. Bachmann, Carsten Putzke, et al.

Applied Physics Letters ARTICLE scitation.org/journal/apl

Controlling superconductivity of $CeIrIn_5$ microstructures by substrate selection

Cite as: Appl. Phys. Lett. **120**, 092601 (2022); doi: 10.1063/5.0082561
Submitted: 16 December 2021 · Accepted: 15 February 2022 ·
Published Online: 2 March 2022

Maarten R. van Delft,[1,a),b)] Maja D. Bachmann,[2,3] Carsten Putzke,[1] Chunyu Guo,[1] Joshua A. W. Straquadine,[1] Eric D. Bauer,[4] Filip Ronning,[4] and Philip J. W. Moll[1,a)]

AFFILIATIONS

[1]Laboratory of Quantum Materials (QMAT), Institute of Materials (IMX), École Polytechnique Fédérale de Lausanne (EPFL), 1015 Lausanne, Switzerland
[2]Max Planck Institute for Chemical Physics of Solids, 01187 Dresden, Germany
[3]Scottish Universities Physics Alliance, School of Physics and Astronomy, University of St. Andrews, St. Andrews KY16 9SS, United Kingdom
[4]Los Alamos National Laboratory, Los Alamos, New Mexico 87545, USA

[a)]**Authors to whom correspondence should be addressed:** maarten.vandelft@ru.nl and philip.moll@epfl.ch
[b)]**Present address:** High Field Magnet Laboratory (HFML—EMFL), Radboud University, Toernooiveld 7, 6525 ED Nijmegen, The Netherlands.

ABSTRACT

Superconductor/metal interfaces are usually fabricated in heterostructures that join these dissimilar materials. A conceptually different approach has recently exploited the strain sensitivity of heavy-fermion superconductors, selectively transforming regions of the crystal into the metallic state by strain gradients. The strain is generated by differential thermal contraction between the sample and the substrate. Here, we present an improved finite-element model that reliably predicts the superconducting transition temperature in $CeIrIn_5$ even in complex structures. Different substrates are employed to tailor the strain field into the desired shapes. Using this approach, both highly complex and strained as well as strain-free microstructures are fabricated to validate the model. This enables a high degree of control over the microscopic strain fields and forms the basis for more advanced structuring of superconductors as in Josephson junctions yet also finds natural use cases in any material class in which a modulation of the physical properties on a chip is desirable.

The local and selective transformation of material properties forms the basis of electronics. In the transistor, for example, electric fields drive the transition between an insulator and a metallic conductor. In correlated electron systems, phase transformations can be driven via relevant tuning parameters, such as strain. In thin film materials, strains caused by mismatch between a substrate and film have been investigated for a long time.[1] Such mismatch strains can either be a nuisance, as a source of dislocations and material incompatibility, or a blessing, leading to desirable band structure modifications. Each film, thus, presents a new challenge in finding the right substrate to achieve the desired level of strain.[2–4] In bulk crystals, however, strain and strain gradients are usually weak. When it is desirable to purposely induce strain, often an elaborate straining apparatus is required.[5,6]

Regardless of whether one is dealing with strain in a thin film or in a bulk crystal, the strain is usually applied globally to the entire film or crystal. Strategies do exist to induce controlled local strains in certain two-dimensional materials,[7,8] but these do not translate well to three-dimensional solids, while a method to control strain locally could enable both novel types of basic science experiments as well as applications. Recently, controlled T_c landscapes imprinted by static strain gradient fields of $CeIrIn_5$ have been demonstrated.[9] The approach exploits the high sensitivity of its superconducting critical temperature, T_c, on directional strain, which translates strain gradients into T_c gradients. Technically, this was achieved by shaping crystal microstructures via focused ion beam (FIB) and by generating complex strain patterns due to differential thermal contraction between the structure and the substrate.

Here, we build on this work and demonstrate improved control over the T_c landscape. The main advances are a refinement of the finite element modeling of strain fields that is now able to predict local T_c

modifications and an exploration of various substrates with differences in the thermal contraction. Consequently, desired T_c landscapes can be reliably predicted and validated by experiment. We continue to focus on the heavy fermion superconductor $CeIrIn_5$,[10] but the principle is materials agnostic and can be used to tailor strain fields in essentially any material. $CeIrIn_5$ is a convenient material, as its superconductivity is highly sensitive to uniaxial strain.[11,12] In particular, the tetragonal compound reacts to strain in a directional way: While compression along the *a*-direction increases T_c, it is reduced by compression along the *c*-direction.

The origin of the strain in our system is illustrated in Fig. 1(a). We fix a crystal slab, which we call a lamella, onto a substrate at room temperature using a thin layer of epoxy. As the sample is cooled to near-zero kelvin, the crystal experiences a different thermal contraction than the substrate, causing strain in the small sample due to its rigid connection to the substrate. This strain is not uniform, but is distributed depending on the shape of the sample that sets the elastic boundary conditions. Using a FIB, we can modify this shape in order to prepare a device suitable for electrical measurements, with a desired strain pattern. As sample and substrate are joined by epoxy glue, the method does not suffer from material incompatibilities that commonly arise from lattice mismatch in epitaxially grown heterostructures. The relaxed structure is glued to the substrate at room temperature where the mechanical bond is formed and then heated to 140 °C to outgas remaining organic solvents before further processing. Strain then arises from differences in thermal contraction when cooling down to low temperatures [see Fig. 1(a)]. The fabrication method of these crystalline structures has been reported elsewhere.[13,14]

The magnitude and spatial distribution of the strain are modeled using finite element simulations implemented in the structural mechanics module of COMSOL multiphysics[9] (see the supplementary material for details). Figures 1(b) and 1(c) display a single-crystal T-shaped sample geometry. As indicated in Fig. 1(b), the central beam guides the current, while the lateral crystal pads serve as voltage contacts. Unavoidably, these contacts also transduce stress into the beam, which then shapes the strain profile [shown in Fig. 1(c) for strain along the a-axis]. This geometry is useful to determine the transport anisotropy in a crystal, as it allows resistance measurements along two different crystallographic axes, in this case the *a*- and *c*-axes of $CeIrIn_5$. The high level of complexity of such a structure is an ideal testbed for simulations, where the mechanical model is used to predict the components of the strain tensor along the *a*- and *c*-axes. We also calculate the other components, but these are small enough to be safely neglected (see the supplementary material, Fig. S1 for an overview of all components).

The overall magnitude of the strain strongly depends on the choice of the substrate material and its thermal contraction. Previous work on $CeIrIn_5$[9] and other materials[15] focused exclusively on sapphire as a substrate, while here we employ various materials to engineer the strain. Sapphire has a small coefficient of thermal expansion ($\alpha = \frac{1}{L}\frac{dL}{dT}$) and, hence, contracts little when cooled down. Combined with the strong contraction of $CeIrIn_5$, this leads to a sizeable strain. For higher strain applications, this can be further enhanced by using fused silica as substrate, a material with even lower α than sapphire ($\alpha_{\text{sapphire}} = 5.4 \times 10^{-6}$ K^{-1} vs $\alpha_{\text{fused silica}} = 0.5 \times 10^{-6}$ K^{-1} at room temperature[16,17]). For low strain applications, on the other hand, it is desirable to use a substrate with α similar to that of the material under study; a convenient option for $CeIrIn_5$ is CaF_2 ($\alpha_{CaF_2} = 18.85 \times 10^{-6}$ K^{-1} at room temperature[18]).

As expected, the choice of the substrate has a significant effect on the strain and T_c is strongly modulated within the structure [Figs. 1(d)–1(f)]. The local T_c is computed from the local ratio of the *c* and *a* lattice parameters, whose dependence has been previously obtained in uniaxial pressure experiments on macroscopic crystals.[11] It is clear that significant variations in T_c exist across any device on sapphire or fused silica, which will certainly affect measurements of these devices, for instance, leading to multiple superconducting transitions seen in electrical measurements. If instead of strain engineering a measurement corresponding to the intrinsic properties of bulk $CeIrIn_5$ is desired, the use of a CaF_2 substrate is expected to reduce this variation to a minimum. As seen in Fig. 1(d), T_c variations in this device on CaF_2 are considerably smaller, of the order of 20 mK.

For an optimal measurement of intrinsic $CeIrIn_5$ along well-defined crystallographic directions, the T_c variations can be further

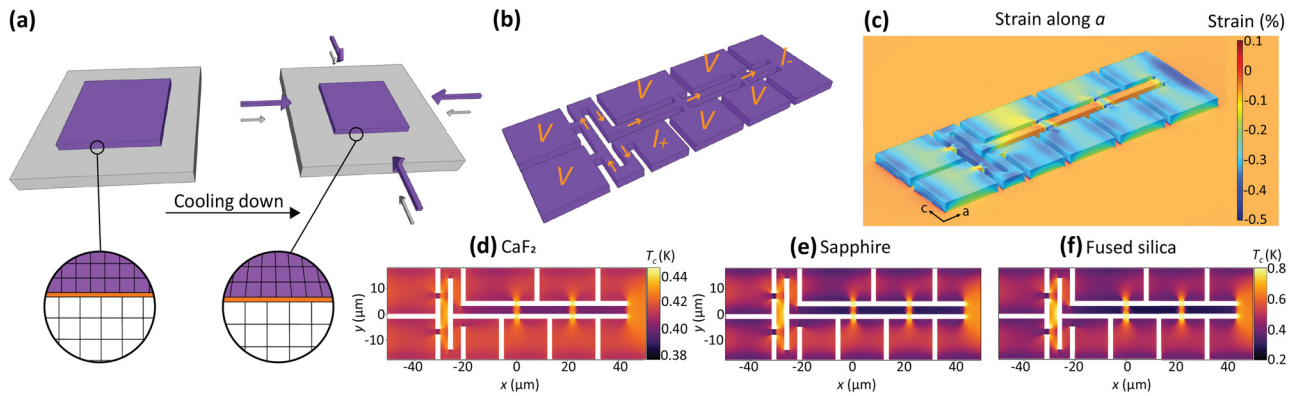

FIG. 1. (a) Illustration of the differential thermal contraction taking place in the $CeIrIn_5$/substrate devices. The crystal (purple) contracts more than the substrate (gray), leading to strain at the interface. The glue layer (brown) buffers any lattice mismatch. (b) Sketch of a T-shaped device geometry. The arrows indicate the current flow between the I_+ and I_- pads. (c) Components of the strain tensor along the *a*-axis, shown on a T-shape device on a sapphire substrate. The variations in the strain patterns in the contact pads are a result of their different lateral dimensions. (d)–(f) Simulated critical temperatures, T_c, of T-shaped devices on different substrate materials: (d) CaF_2, (e) sapphire, and (f) fused silica. T_c is calculated in the horizontal center plane of the devices, and the scale bar shown in (f) applies to (e) and (f).

reduced by adapting the geometry. Here, it is important to note that larger T_c variations arise near edges and corners. It is, therefore, important to avoid having those near the sections of the device that are being measured, i.e., between the contacts. Naturally, the contact connections themselves are points that transduce strain. We, therefore, further optimize the design to reduce T_c variation near the contacts: The corners are rounded and the contact connections are softened by elongating and thinning them.

Figure 2 summarizes the best attempt at such a low-strain device. Our simulations of this device show a maximal variation in T_c of approximately 5 mK across the longer a-leg (R_{12}) of the device and 10 mK across the shorter b-leg (R_{56}). Experimentally, we observe a sharp superconducting transition in the a-leg with an onset temperature of 410 mK, in good agreement with reports of bulk $CeIrIn_5$.[10,19,20] The transition in the b-leg occurs at a slightly higher temperature, with an onset of 440 mK. This small deviation, in addition to the slight deviation above T_c, suggests a reorientation of the effective current path as the residual strain inhomogeneity is translated to variations in the local T_c. Above 570 mK and below 400 mK, the *a* and *b* resistivities overlap as expected and both reach zero at $T_c^0 = 386$ mK.

The elimination of strain demonstrated here paves the way toward finite size studies of confined heavy-fermion conductors without the additional worries of strain effects. Yet tailoring strong strain fields also enables novel functionality, such as intentionally creating sections of devices with enhanced or suppressed T_c. These approaches will be based on the high-strain substrate fused silica. The shape of the microstructure can focus the strain into a small area, which happens most effectively in a bridge-like structure: a thin bar between two large blocks of crystal. Our results for a device of this type are summarized in Fig. 3.

The device shown in Fig. 3(a) has a 7 μm long and 2 μm wide bridge in which superconductivity is expected to be fully suppressed, as suggested by simulations of this device [see Fig. 3(b)]. Experimentally, this is indeed what we observe. In Fig. 3(c), we show the measured resistivity of this device as a function of temperature. Around 500 mK, a transition takes place arising from the bulk slabs outside the bridge. Below this temperature, the resistivity gradually decreases until it saturates at around 0.25 $\mu\Omega$ cm, a value in good agreement with previous reports in the normal state.[9] The gradual decrease in resistivity is likely due to a combination of the usual metallic conductivity of $CeIrIn_5$ above T_c and the region of partially suppressed superconductivity extending a few μm from either end of the bridge.

The structure shown in Fig. 3 is rather simple, and the geometric factors of length, width, and thickness of the bridge dominantly set its T_c. Yet further, the depth and shape of the cuts made into the lamella on either side of the bridge play an important role as well as they are important in setting the elastic boundary condition for the problem. Cutting deep into the substrate and cutting at a larger opening angle both increase the strain experienced by the bridge. Generally, direct contact between the bridge and the epoxy on the substrate is not beneficial and a stronger strain can be achieved by undercutting it. In devices with fully suppressed superconductivity, a compressive c-axis strain of approximately 0.6% is typically the main driving factor, while the a-axis strain of about 0.5% has an opposite sign between the in- and out-of-plane directions and, therefore, has only minor impact on T_c.

Having demonstrated both extremes of our technique, low strain and high strain, we now turn to the design of complex strain and T_c patterns. This serves as a demonstration of the engineering capabilities of the approach yet also tests our model over a wide range of temperatures. To this end, we have fabricated an approximately 4 μm thick semi-circular structure shown in Fig. 4(a). The direction of the strain relative to the crystallographic axes varies continuously along the

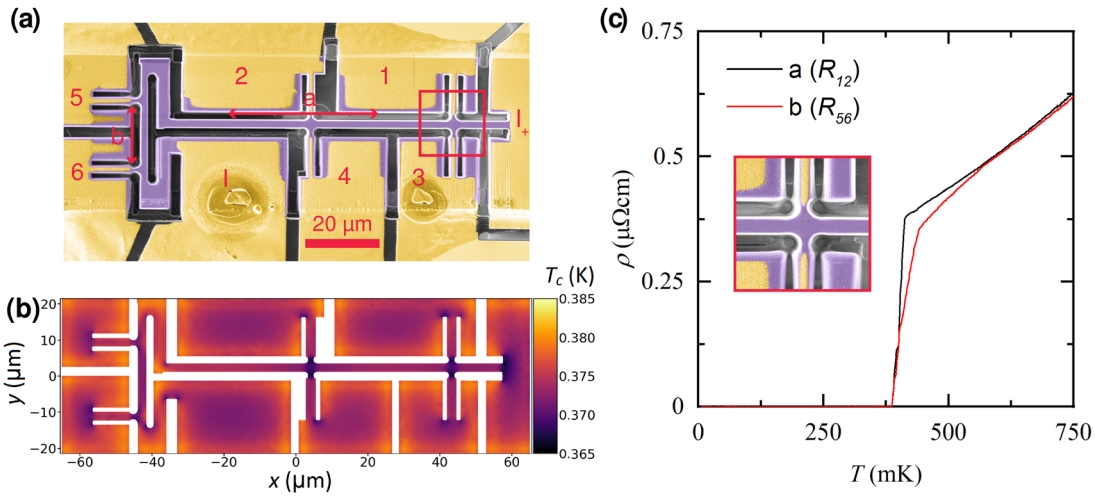

FIG. 2. (a) False-color SEM image of a strain-minimizing T-shape device of $CeIrIn_5$ on a CaF_2 substrate. The crystal itself has been colored purple, while the Ti/Au contacts are shown as yellow. For our experiment, a current is passed between the contacts labeled $I_\pm$, and voltages are measured between contacts 1–2, and 5–6. (b) Simulated T_c map of the device shown in (a). Variations in T_c across the active sections of this device are limited to approximately 5 mK. (c) Resistivity measurements of the long (*a*) and short (*b*) legs of the device, showing the superconducting transition in agreement with a nearly unstrained device. For both legs, a state of zero resistance is reached at $T_c^0 = 386$ mK. The first onset of a superconducting transition takes place at $T_c^{onset} = 410$ mK for the a-leg and 440 mK for the b-leg. Inset: enlarged view of the marked section in (a), showing the rounded corners of this design.

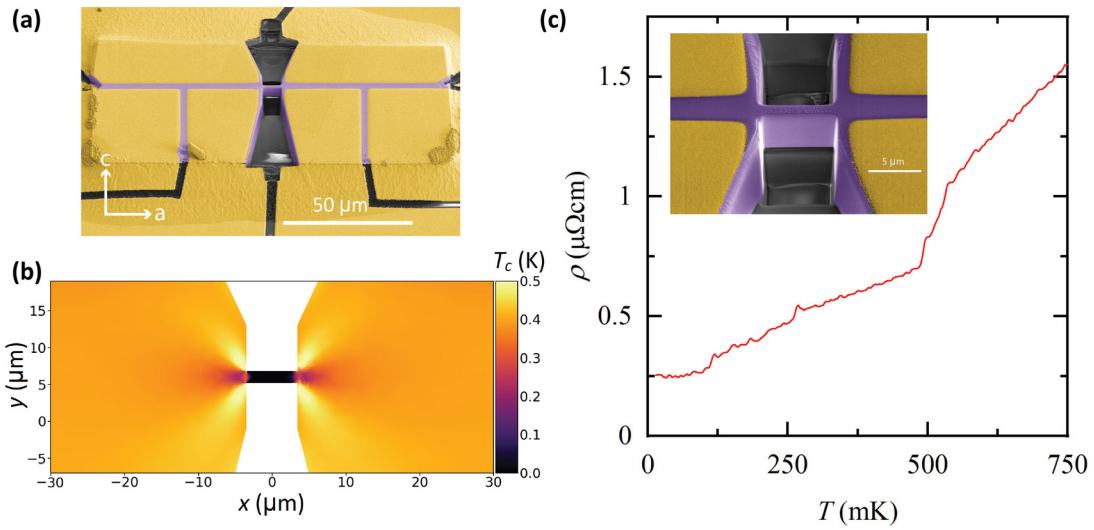

FIG. 3. (a) False-color SEM image of a $CeIrIn_5$ device on a fused silica substrate designed to maximize the strain in one section. (b) Simulated T_c map of the device shown in (a). The bridge section in the center has $T_c = 0$ K. (c) Resistivity measurement through the bridge section of the device (shown in the inset). The bridge does not become superconducting but maintains a resistivity comparable to previous reports[9] down to the base temperature of our experiment.

circle, leading to either suppression or enhancement of T_c in different sections. This is shown by our simulation, in Fig. 4(b).

In Fig. 4(c), we show the measured resistances between each of the pairs of adjacent contacts to the device. The results are in good agreement with our predictions and are symmetric between the left and right sides of the device, thereby confirming the accurate crystallographic alignment. As expected, the section between contacts 5 and 6 shows the lowest T_c, below the minimal temperature accessible to the measurement, and the sections 0–1 and 10–11 show the highest T_c, about twice the value of bulk $CeIrIn_5$.

The overall agreement between our simulations and experiment is demonstrated by Fig. 4(d), where we have included experimental data and simulations from multiple sections of 8 devices. The good agreement confirms the validity of the model and that T_c landscapes

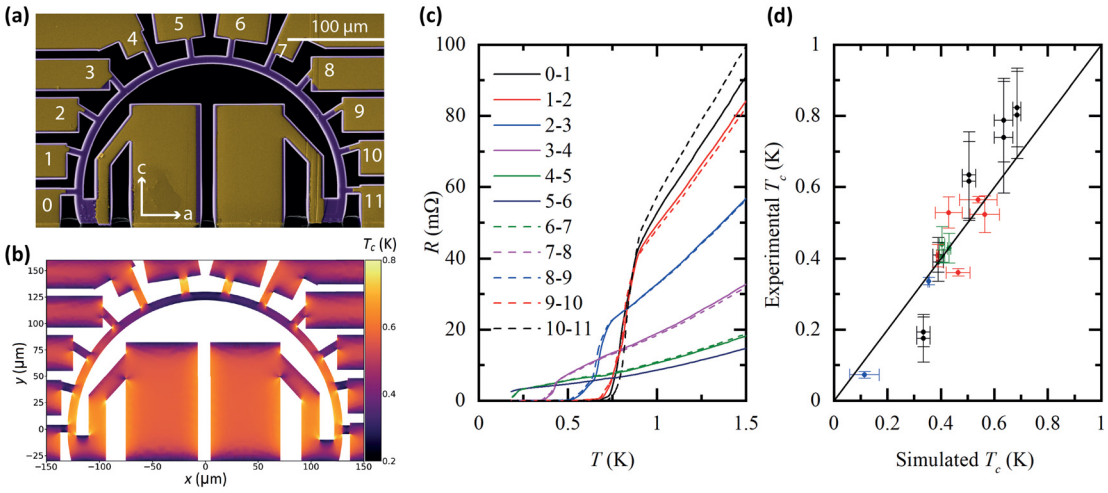

FIG. 4. (a) False-color SEM image of a circular device on a sapphire substrate, designed to exhibit a broad range of critical temperatures. The voltage contacts of the device are numbered 0 to 11. (b) Simulated T_c map of the device shown in (a). (c) Experimental superconducting transitions measured in the device shown in (a). The numbers in the legend correspond to the pairs of contacts measured for the respective curves. Note that the contact pairs close to the current contacts slightly differ in the normal state resistance owing to the imperfect flow homogenization at this point of the semi-circle. This effect does not change the apparent T_c. (d) Experimental vs simulated critical temperatures for several devices. The straight line represents perfect agreement of simulation and experiment. Black dots were extracted from the semi-circular device, red and blue dots from the bulk and bridge sections of bridge-style devices, respectively, and green dots from low-strain devices. Device sections with $T_c = 0$ K are not included, as these typically have simulated critical temperatures slightly below zero, resulting from the very high strain. Vertical error bars are determined from the width of the measured transitions and horizontal error bars from the range of simulated T_c values over the relevant device sections.

can be selectively written into superconductors using the FIB. The remaining discrepancies can be well explained by unintentional deviations of the real devices from the targeted models. For instance, the simulations assume that all devices are perfectly flat on the epoxy layer at exact crystallographic orientation, while in practice this alignment will be imperfect on the order of a percent. Additionally, the apparent value of the resistance may also be influenced by parallel conductance paths through redeposited material.

In conclusion, we have demonstrated microscopic control over the superconducting critical temperature T_c of $CeIrIn_5$ over a range from 0 K to at least twice the bulk T_c, by making use of the thermal contraction of different substrate materials and by careful device design. We, additionally, demonstrate the validity of finite element simulations for the prediction of T_c, enabling the design of devices with particular T_c landscapes as desired. With this, we have laid the groundwork for the design and fabrication of functional devices. The methodology presented here is materials agnostic as no structural or chemical compatibility between the substrate and sample is required and can be used to tailor strain fields in them on the micrometer scale. In the future, such exploitation of strain-induced phase transformations in strongly correlated materials will surely enable new types of spatially modulated structures.

The supplementary material includes additional details on the device fabrication and simulations. Material properties used for the simulations are listed, and three figures with detailed simulation results are given.

M.R.v.D. acknowledges funding from the Rubicon research program with Project No. 019.191EN.010, which is financed by the Dutch Research Council (NWO). M.D.B. acknowledges Engineering and Physical Sciences Research Council (EPSRC) for Ph.D. studentship support through Grant No. EP/L015110/1. This project received funding by the Swiss National Science Foundation (Grants No. PP00P2_176789 and 206021_189675). Work at Los Alamos was carried out under the auspices of the U.S. Department of Energy, Office of Science, Basic Energy Sciences, Materials Sciences and Engineering Division.

AUTHOR DECLARATIONS

Conflict of Interest

The authors declare no conflicts of interest.

DATA AVAILABILITY

The data that support the findings of this study are openly available in the Zenodo repository at https://doi.org/10.5281/zenodo.5785684 (Ref. 21).

REFERENCES

[1]G. G. Stoney, "The tension of metallic films deposited by electrolysis," Proc. R. Soc. A **82**, 553 (1909).
[2]G. Abadias, E. Chason, E. Keckes, M. Sebastiani, G. B. Thompson, E. Barthel, G. L. Doll, C. E. Murray, C. H. Stoessel, and L. Martinu, "Review Article: Stress in thin films and coatings: Current status, challenges, and prospects," J. Vacuum Sci. Technol., A **36**, 020801 (2018).
[3]A. M. Engwall, Z. Rao, and E. Chason, "Origins of residual stress in thin films: Interaction between microstructure and growth kinetics," Mater. Des. **110**, 616–623 (2016).
[4]F. Motazedian, J. Zhang, Z. Wu, D. Jiang, S. Sarkar, M. Martyniuk, C. Yan, Y. Liu, and H. Yang, "Achieving ultra-large elastic strains in Nb thin films on NiTi phase-transforming substrate by the principle of lattice strain matching," Mater. Des. **197**, 109257 (2021).
[5]I. Kostylev, S. Yonezawa, and Y. Maeno, "Piezoelectric-based uniaxial strain cell with high strain throughput and homogeneity," J. Appl. Phys. **125**, 082535 (2019).
[6]C. W. Hicks, M. E. Barber, S. D. Edkins, D. O. Brodsky, and A. P. Mackenzie, "Piezoelectric-based apparatus for strain tuning," Rev. Sci. Instrum. **85**, 065003 (2014).
[7]M. Foerster, E. Menéndez, E. Coy, A. Quintana, C. Gómez-Olivella, D. Esqué De Los Ojos, O. Vallcorba, C. Frontera, L. Aballe, J. Nogués, J. Sort, and I. Fina, "Local manipulation of metamagnetism by strain nanopatterning," Mater. Horiz. **7**, 2056–2062 (2020).
[8]M. Bollani, D. Chrastina, L. Gagliano, L. Rossetto, D. Scopece, M. Barget, V. Mondiali, J. Frigerio, M. Lodari, F. Pezzoli, F. Montalenti, and E. Bonera, "Local uniaxial tensile strain in germanium of up to 4% induced by SiGe epitaxial nanostructures," Appl. Phys. Lett. **107**, 083101 (2015).
[9]M. D. Bachmann, G. M. Ferguson, F. Theuss, T. Meng, C. Putzke, T. Helm, K. R. Shirer, Y.-S. Li, K. A. Modic, M. Nicklas, M. König, D. Low, S. Ghosh, A. P. Mackenzie, F. Arnold, E. Hassinger, R. D. McDonald, L. E. Winter, E. D. Bauer, F. Ronning, B. J. Ramshaw, K. C. Nowack, and P. J. W. Moll, "Spatial control of heavy-fermion superconductivity in $CeIrIn_5$," Science **366**, 221–226 (2019).
[10]C. Petrovic, R. Movshovich, M. Jaime, P. G. Pagliuso, M. F. Hundley, J. L. Sarrao, Z. Fisk, and J. D. Thompson, "A new heavy-fermion superconductor $CeIrIn_5$: A relative of the cuprates?," Europhys. Lett. **53**, 354–359 (2001).
[11]O. M. Dix, A. G. Swartz, R. J. Zieve, J. Cooley, T. R. Sayles, and M. B. Maple, "Anisotropic dependence of superconductivity on uniaxial pressure in $CeIrIn_5$," Phys. Rev. Lett. **102**, 197001 (2009).
[12]N. Oeschler, P. Gegenwart, M. Lang, R. Movshovich, J. L. Sarrao, J. D. Thompson, and F. Steglich, "Uniaxial pressure effects on $CeIrIn_5$ and $CeCoIn_5$ studied by low-temperature thermal expansion," Phys. Rev. Lett. **91**, 076402 (2003).
[13]P. J. Moll, "Focused ion beam microstructuring of quantum matter," Annu. Rev. Condens. Matter Phys. **9**, 147–162 (2018).
[14]P. J. Moll, B. Zeng, L. Balicas, S. Galeski, F. F. Balakirev, E. D. Bauer, and F. Ronning, "Field-induced density wave in the heavy-fermion compound $CeRhIn_5$," Nat. Commun. **6**, 6663 (2015).
[15]M. D. Bachmann, A. L. Sharpe, A. W. Barnard, C. Putzke, M. König, S. Khim, D. Goldhaber-Gordon, A. P. Mackenzie, and P. J. W. Moll, "Super-geometric electron focusing on the hexagonal Fermi surface of $PdCoO_2$," Nat. Commun. **10**, 5081 (2019).
[16]J. W. Ekin, *Experimental Techniques for Low-Temperature Measurements: Cryostat Design, Material Properties and Superconductor Critical-Current Testing* (Oxford University Press, 2006).
[17]T. A. Hahn and R. K. Kirby, "Thermal Expansion of Fused Silica from 80 to 1000 K - Standard Reference Material 739," AIP Conf. Proc. **3**, 13 (1972).
[18]D. N. Batchelder and R. O. Simmons, "Lattice constants and thermal expansivities of silicon and of calcium fluoride between 6 and 322 K," J. Chem. Phys. **41**, 2324–2329 (1964).
[19]Y. Chen, W. B. Jiang, C. Y. Guo, F. Ronning, E. D. Bauer, T. Park, H. Q. Yuan, Z. Fisk, J. D. Thompson, and X. Lu, "Reemergent superconductivity and avoided quantum criticality in Cd-doped $CeIrIn_5$ under pressure," Phys. Rev. Lett. **114**, 146403 (2015).
[20]R. Borth, E. Lengyel, P. G. Pagliuso, J. L. Sarrao, G. Sparn, F. Steglich, and J. D. Thompson, "Heat capacity of the heavy fermion superconductor $CeIrIn_5$ under hydrostatic pressure," Phys. B: Condens. Matter **312–313**, 136–137 (2002).
[21]M. van Delft, M. Bachmann, C. Putzke, C. Guo, J. Straquadine, E. Bauer, F. Ronning, and P. Moll (2021). "Controlling superconductivity of CeIrIn5 microstructures by substrate selection," Zenodo. https://doi.org/10.5281/zenodo.5785684